EAI Endorsed Transactions
on Digital Transformation of Industrial Processes Research Article EAI.EU

Analysis of Temperature Distribution During Grinding with Variable Wheel Feed

R. Strelchuk[1,*], I. Riabenkov [2]

[1] Simon Kuznets Kharkiv National University of Economics, Nauky Ave., 9a, Kharkiv, 61166, Ukraine
[2] National Aerospace University "Kharkiv Aviation Institute", 17, Vadym Manko St., 61070 Kharkiv, Ukraine

Abstract

INTRODUCTION: Creep-feed grinding of ultrahard cutting tool materials such as cermet presents significant thermal challenges due to extended contact arc lengths between wheel and workpiece combined with low thermal conductivity of the workpiece material. These conditions lead to dramatic temperature rises and potential burnout phenomena that compromise grinding quality and wheel life.
OBJECTIVES: This study aims to experimentally investigate grinding temperature distribution within the contact arc during creep-feed grinding of cermet workpieces, identify critical burnout conditions, and determine optimal grinding parameters to enhance cooling effectiveness and prevent thermal damage.
METHODS: Grinding temperature measurements were conducted using an embedded thermocouple method during creep-feed grinding of Ti(C,N) cermet alloy with hybrid-bonded diamond wheels. Temperature distributions along the contact arc were measured across various combinations of worktable speeds (40–80 mm/min), wheel speeds (14.7–62.9 m/s), and wheel diameters (140 mm and 200 mm). The onset and progression of burnout phenomena were systematically documented and analyzed.
RESULTS: Experimental results revealed that burnout occurs when grinding temperature reaches approximately 150°C, causing abrupt temperature increases exceeding 400°C. Burnout initiates at the rear of the contact arc and progressively extends throughout the grinding zone. A critical worktable speed exists above which burnout occurs under constant depth of cut and wheel speed conditions. Smaller wheel diameters and optimized wheel speeds significantly improve cooling effectiveness. At wheel speed of 41.9 m/s, burnout was nearly eliminated with maximum temperatures maintained below 150°C along the entire contact arc, resulting in reduced grinding forces and wheel wear.
CONCLUSION: The research demonstrates that strategic control of grinding parameters, particularly wheel speed optimization and wheel diameter selection, effectively prevents burnout and enhances cooling performance in creep-feed grinding of difficult-to-grind cermet materials. Higher wheel speeds improve grinding fluid circulation and cooling effectiveness up to an optimal threshold, beyond which excessive heat generation and reduced fluid supply negate these benefits.

Keywords: grinding temperature distribution, burnout phenomenon, film boiling, cermet machining, creep-feed grinding optimization, hybrid-bonded diamond wheel, thermal management.

Received on 26 January 2026, accepted on 25 February 2026, published on 27 February 2026

doi: 10.4108/dtip.11703

1. Introduction

The manufacturing of precision cutting tools for high-speed machining applications has experienced substantial growth in recent decades, driven by the increasing adoption of advanced machining centers in industrial production.

*Corresponding author. Email: r.m.strelchuk@gmail.com

Throwaway cutting inserts and chip breakers, fabricated from ultrahard materials such as tungsten carbide, cermet (ceramic-metal composites), and advanced ceramics, have become essential components in modern manufacturing processes [1]. These materials exhibit exceptional hardness and wear resistance, properties that are critical for cutting tool performance but simultaneously present significant challenges during their own fabrication through grinding operations [2].

The grinding of ultrahard cutting tool materials is characterized by inherent difficulties arising from their mechanical and thermal properties. High grinding forces, excessive heat generation at the grinding interface, thermal crack formation on machined surfaces, and accelerated grinding wheel wear constitute primary concerns that limit productivity and product quality. Among these materials, cermet alloys based on Ti(C,N) compositions represent particularly challenging workpieces due to their extremely low thermal conductivity combined with high hardness, making them prone to thermal damage during grinding operations [3].

In response to these manufacturing challenges, considerable research efforts have been directed toward developing specialized grinding tools and optimizing process parameters for high-efficiency grinding of ultrahard materials. The development of advanced hybrid-bonded diamond wheels has emerged as a promising solution, combining the advantages of different bonding systems to achieve superior performance in demanding grinding applications. Previous investigations into the fundamental wear mechanisms of diamond wheels during cermet grinding have revealed important insights regarding process optimization. Comparative studies examining creep-feed grinding versus conventional pendulum grinding modes, conducted under conditions of constant specific material removal rate, have demonstrated that creep-feed grinding can achieve reduced wheel wear despite employing significantly greater depths of cut.

However, creep-feed grinding introduces distinct thermal management challenges that require careful consideration. The extended contact arc length between the grinding wheel and workpiece in creep-feed mode creates conditions conducive to substantial heat accumulation within the grinding zone. This thermal characteristic is further exacerbated when processing cermet materials, whose low thermal conductivity restricts heat dissipation and promotes temperature elevation. Maintaining controlled grinding temperatures is therefore essential for preserving favorable grinding conditions and achieving acceptable surface quality. Additionally, diamond abrasive grains, despite their exceptional hardness, exhibit degradation of mechanical properties at elevated temperatures, necessitating comprehensive understanding of grinding temperature characteristics before meaningful analysis of wheel wear mechanisms can be undertaken.

The scientific literature contains several notable contributions addressing grinding temperatures and thermal damage in precision grinding operations. Comprehensive thermal modeling approaches have been developed that incorporate the interacting effects of global and local thermal phenomena while accounting for grinding fluid behavior [4]. Such models have been applied to analyze heat distribution patterns and temperature fields within the contact arc during creep-feed grinding [5]. Specialized heat transfer models incorporating film boiling phenomena have been formulated to predict temperature distributions along the grinding contact zone. Theoretical investigations have pursued exact solutions for surface temperature evolution, examining the influence of heat generation location, whether at abrasive grain wear flats or within chip shear planes [6].

Despite these theoretical advances, a significant gap exists in experimental validation of predictive models, primarily due to practical difficulties in measuring temperatures under actual grinding conditions. This limitation is particularly evident in the context of creep-feed grinding operations, where empirical data regarding grinding temperatures, burnout (film boiling) phenomena, and cooling effectiveness of grinding fluids remain scarce [7]. The present investigation addresses this deficiency through systematic experimental study of temperature distributions within the grinding contact arc during creep-feed grinding of cermet workpieces.

This research employs Ti(C,N)-based cermet from the titanium nitride series as the workpiece material, representing one of the most difficult-to-grind materials among throwaway cutting tool inserts currently in industrial use. Through direct temperature measurement using thermocouple techniques, the temperature distribution along the contact arc between the grinding wheel and cermet workpiece is experimentally determined. The cooling effectiveness of grinding fluid under various operating conditions is evaluated and quantified. The study identifies and characterizes the burnout phenomenon of grinding fluid within the contact zone, documenting its initiation and progression during the grinding process [8].

Furthermore, the influences of critical process parameters, including wheel peripheral speed, worktable feed speed, and wheel diameter, on grinding temperature characteristics are systematically investigated. Based on these experimental findings, optimal grinding conditions from a thermal management perspective are proposed to enable efficient and reliable grinding of cermet materials while minimizing thermal damage and wheel wear.

2. Research Methodology

The experimental investigation of grinding temperatures was conducted using an embedded thermocouple measurement technique, which enables direct monitoring of temperature variations at the grinding interface [9, 10]. The measurement system configuration and workpiece assembly are illustrated in Figure 1. The thermocouple junction was created through a specialized workpiece construction method designed to position the temperature-sensing element precisely at the ground surface [11, 12].

The workpiece assembly consisted of two cermet specimens with dimensions of 12.7 mm × 1.0 mm, featuring carefully prepared and polished end surfaces to ensure intimate contact. An iron foil with thickness of 0.1 mm and a constantan wire with diameter of 0.076 mm were positioned between the cermet pieces, separated by a thin mica insulating sheet of 0.01 mm thickness. These components were compressed together under controlled pressure to form a composite workpiece structure. Prior to grinding operations, electrical resistance measurements between the iron foil and constantan wire confirmed complete electrical isolation, with resistance values exceeding 500 MΩ, thereby ensuring no premature thermocouple junction formation.

During the grinding process, material removal from the workpiece surface progressively exposed the embedded iron foil and constantan wire. At the moment when both conductive elements became simultaneously exposed on the ground surface, a functional iron-constantan thermocouple junction was established in situ. This hot junction, created directly at the grinding interface, enabled real-time temperature measurement of the workpiece surface as it traversed through the grinding contact arc.

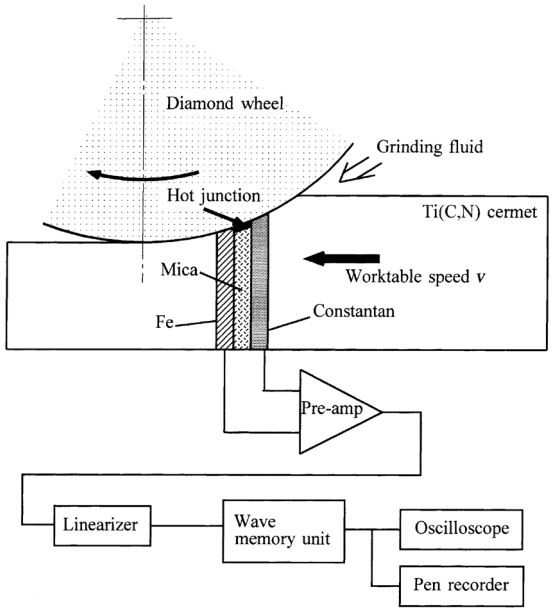

Figure 1. Apparatus for measuring grinding temperature

The thermocouple output signals were processed through a multi-stage signal conditioning system to ensure accurate temperature measurement. The iron-constantan (Type J) thermocouple junction was verified prior to each experimental session through a standard static calibration procedure using a reference thermometer immersed in a temperature-controlled bath across the relevant measurement range (25–500°C). The precision differential amplifier employed to enhance the thermoelectric signal-to-noise ratio was calibrated against known reference voltages corresponding to established iron-constantan EMF–temperature relationships per ITS-90 standards. The linearization circuit was verified to compensate accurately for the nonlinear voltage-temperature characteristic of the iron-constantan system. Electrical isolation between the iron foil and constantan wire prior to grinding was confirmed by resistance values exceeding 500 MΩ, ensuring no spurious junction formation before the grinding surface was reached. These calibration steps collectively ensured that the thermocouple measurements presented in Figures 2–7 accurately reflect actual grinding interface temperatures, and that the critical threshold of ~150°C associated with burnout onset was reliably determined and reproducible across all experimental trials.

The grinding experiments were performed under carefully controlled conditions as specified in Table 1. A hybrid-bonded diamond grinding wheel, specifically developed for high-efficiency machining of ultrahard materials, served as the cutting tool. Two wheel sizes were employed in the investigation: a primary wheel of 200 mm diameter × 6 mm thickness × 3 mm bore (SD270-100-HB designation), and a secondary wheel of 140 mm diameter with identical thickness and bore dimensions. The hybrid bonding system combines the advantages of both resinoid and vitrified bonds, providing enhanced grain retention while maintaining sharp cutting characteristics essential for cermet grinding.

Table 1. Grinding conditions

Parameter	Table column heading
Grinding wheel	Hybrid-bonded diamond wheel SD270-100-HB
Workpiece material	Cermet—Ti(C,N) alloy 50.8 L×1.0 W mm; 25.4 L×1.0 W mm
Wheel depth of cut	0.5 mm
Worktable speed	40–80 mm/min
Wheel peripheral speed	14.7, 29.3, 41.9, 62.9 m/s
Grinding fluid	Chemical solution type synthetic coolant, 25 l/min

The workpiece material consisted of Ti(C,N) cermet alloy specimens prepared in two standard lengths: 50.8 mm × 1.0 mm for general grinding trials, and 25.4 mm × 1.0 mm for specific parametric studies. The thermocouple-embedded workpiece configuration, as previously described, was utilized exclusively during temperature measurement phases to avoid unnecessary complexity in force and wear measurement trials.

Creep-feed grinding operations were conducted with a constant wheel depth of cut of 0.5 mm, representing a substantial engagement depth characteristic of high-efficiency grinding processes. Worktable feed speeds were systematically varied across the range of 40 to 80 mm/min to investigate the influence of material removal rate on thermal behavior. Wheel peripheral speeds spanned a wide

range from 14.7 m/s to 62.9 m/s, encompassing both conventional and high-speed grinding regimes. This comprehensive speed range enabled investigation of cooling effectiveness across different kinematic conditions. Grinding fluid delivery was accomplished through a high-pressure supply system utilizing three precision nozzles positioned to provide fluid access from multiple directions: one nozzle directed toward the front of the contact arc (grinding fluid entry side), and two additional nozzles positioned laterally to ensure complete coverage of the grinding zone. The grinding fluid employed was a chemical solution type synthetic coolant, supplied at a volumetric flow rate of 35 liters per minute to ensure adequate fluid availability at the grinding interface.

Wheel conditioning operations, consisting of truing and dressing procedures, were systematically performed using a rotating cup-type truer equipped with silicon carbide abrasive wheels. These conditioning operations were executed whenever grinding parameters were modified to ensure consistent wheel topography across all experimental trials. The truing tool configuration and operational parameters are detailed in Table 2.

Table 2. Wheel truing and dressing conditions

Parameter	Table column heading
Truing tool	SiC cup wheel, 90D × 10W mm
Truer peripheral speed	134 m/min
Wheel peripheral speed	314 m/min
Truer feed rate	100 mm/min
Depth of cut per pass	0.02 mm
Truing fluid	Water, 0.7 ml/min

The truing apparatus consisted of a compact cup wheel truer mounted directly on the grinding machine worktable, enabling in-situ wheel conditioning without workpiece removal. Two grades of silicon carbide cup wheels were employed: GC80H10V for aggressive material removal during initial truing, and GC280H10V for final dressing to achieve desired surface finish on the wheel working surface [13, 14]. The truer rotated at a peripheral speed of 134 m/min while the grinding wheel maintained a speed of 314 m/min, creating optimal cutting conditions for effective grain exposure. Truing operations proceeded at a feed rate of 100 mm/min with a conservative depth of cut of 0.02 mm per pass to minimize thermal damage to the wheel bond structure. Minimal water application at 0.7 ml/min provided sufficient lubrication while avoiding excessive fluid that could interfere with the truing mechanism.

3. Result and Discussion

Figure 2 shows an example of the signal from the thermocouple. The waveform is obviously composed of a smooth triangular curve and sharp pulses. The smooth waveform was considered to indicate the grinding temperature θ in the wheel contact area, and the impulse signals to indicate the grinding temperature of individual grains. In this paper, the grinding temperature θ that leads to thermal damage and the change of θ along the contact arc (grinding temperature distribution) are discussed. Here, the value of θ is defined as the increase in temperature of the workpiece from that prior to grinding (approximately 25°C).

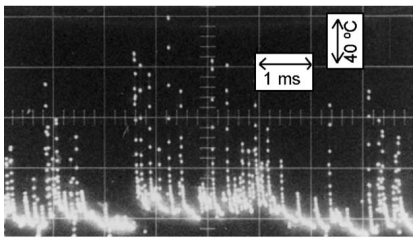

Figure 2. Apparatus for measuring grinding temperature Typical traces of grinding temperature signal (D = 200 mm, Δ = 0.5 mm, V = 14.7 m/s, v = 80 mm/min)

Figure 3 (a)-(c) illustrate the changes in the grinding temperature distribution along the contact arc with increasing material removal volume per unit grinding width. The waveforms correspond to the position of the contact arc between wheel and workpiece. As is evident from Figure 3 (a), at the beginning of the grinding period, the entire area of the contact arc is below 100°C and is cooled efficiently. However, after only a short period of grinding, the temperature distribution changes noticeable, as shown in Figure 3 (b) where high temperature peaks appear sporadically from the center of the contact arc towards the end at part B [15]. It is believed that film boiling of the grinding fluid in the contact arc and the subsequent deterioration of heat transmission are responsible for the elevated temperatures. This phenomenon is known as ‘‘burnout’’ [16]. As grinding progresses, burnout occurs over almost the entire area, except for front part A of the contact arc, as shown in Figure 3 (c). This state persisted for the remainder of the test.

The observed progression of temperature distribution and the onset of burnout in the contact arc can be physically explained by considering the heat transfer characteristics of the system. The thermal behavior observed in this study is physically interpretable through the Péclet number (Pe = V· L_b / α, where V is wheel peripheral speed, L_b is the contact arc length, and α is the thermal diffusivity of the workpiece material). For the Ti(C,N) cermet employed, the extremely low thermal conductivity (~7–10 W/m·K) yields high Péclet numbers even at modest wheel speeds, confirming that heat dissipation through the workpiece is severely limited and that surface temperature is primarily

governed by convective cooling via the grinding fluid. This is consistent with burnout occurring at relatively low absolute temperatures (~150°C). The transition from burnout to non-burnout conditions observed at V = 41.9 m/s is further interpretable in terms of the heat flux ratio between fluid-side convection and grinding-arc heat generation, where increased wheel velocity enhances fluid entrainment and effective heat removal.

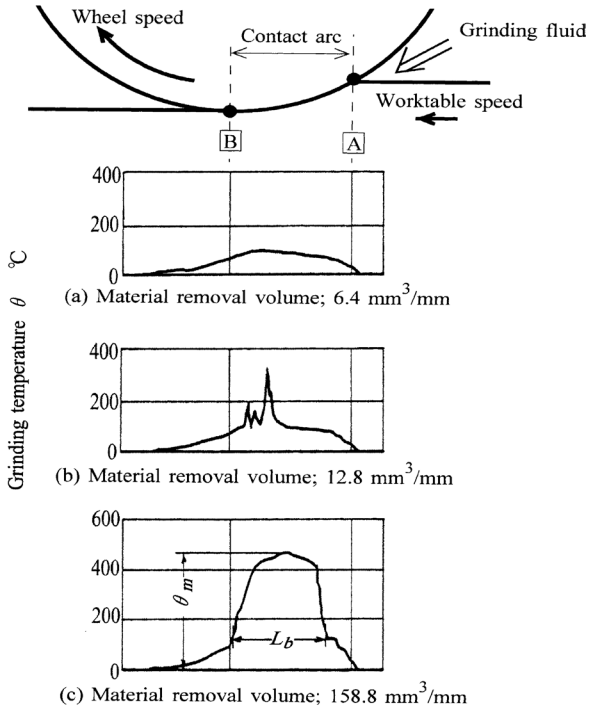

Figure 3. Changes in grinding temperature distribution along contact arc

From these figures, it is evident that the burnout in this experiment occurred when θ reached approximately 150°C. Once burnout occurs, θ in that section increases to over 400°C, and taking the grinding point temperature into consideration, will reach 500-600°C or more. In this region, there is little cooling effect from the grinding fluid, and it is easy to predict that a similar state to dry grinding prevails in spite of the fact that wet grinding is being attempted. Deterioration of both the mechanical strength of the diamond abrasive grains and the gripping strength of the bonding material of the wheel is to be expected. Further, it is conceivable that the grain depth of cut might rapidly increase due to thermal expansion of the workpiece near the grinding point [17]. Under such conditions the fracture and release of the abrasive grains will increase, and so there will be a danger of a rapid increase in the grinding force and thus abnormal wear of the wheel. Therefore, for evaluation of the cooling effect of grinding fluid in the contact arc, the maximum value of θ (defined as maximum grinding temperature θ_m) and the contact arc length where burnout occurred (defined as burnout length L_b) are considered, and the effect of grinding conditions will be discussed in the next section. The grinding temperature distribution along the contact arc was compared with that calculated by Jen and Lavine and under creed-feed grinding conditions under which film boiling occurs [18]. It is interesting to note that wave form of the calculated results agrees well with the experimental data (see Figure 3(c)) and this model can successfully estimate the abrupt temperature transition due to film boiling.

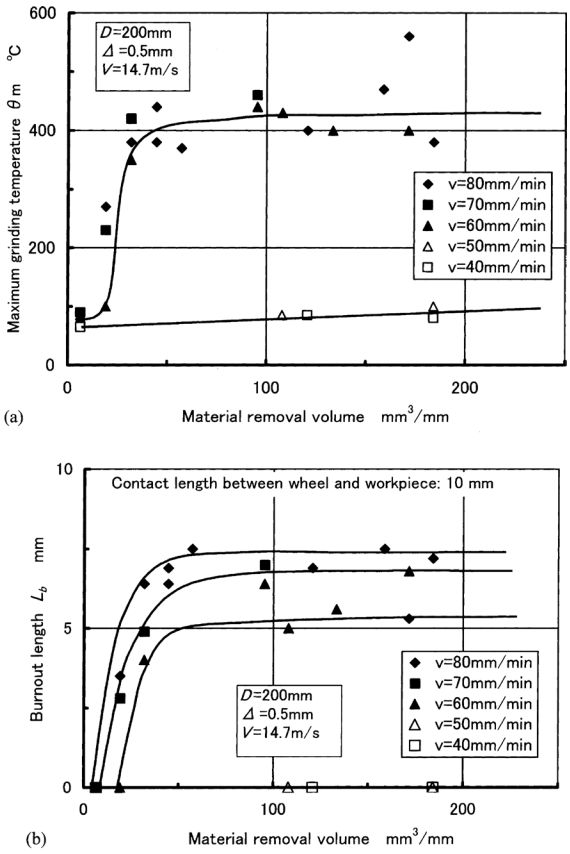

Figure 4. Influence of worktable speed v on maximum grinding temperature θ_m and burnout length L_b for wheel diameter D = 200 mm. (a) Changes in maximum grinding temperature with material removal volume. (b) Changes in burnout length with material removal volume

The maximum grinding temperature θ_m and the burnout length L_b were measured at several worktable speeds and a constant wheel speed of 14.7 m/s. The results are shown in Figure 4. After grinding approximately 40 mm³/mm at a worktable speed of $v \geq 60$ mm/min, burnout occurs and θ_m reaches 400°C or more, as shown in Figure 4 (a). At $v \leq 50$ mm/min, regardless of material removal volume, burnout never occurs and θ_m remains below 100°C. This is because of the decrease in average grinding power per unit area of the contact arc at lower worktable speeds [19]. Thus, when

the depth of cut and wheel speed V are set constant, it is clear that a critical worktable speed exists, above which burnout occurs.

Burnout length L_b rapidly increases with material removal volume and reaches a constant value. The greater the value of v, the greater the burnout length will be. At $v \leq 50$ mm/ min, L_b is 0. In this experiment, the length of the region where the cooling effect of grinding fluid exists is about 3–4 mm from the fluid supply side A (approximately 30– 40% of the total length of the contact arc).

It is believed that the supply of grinding fluid is improved by shortening the contact arc length. Therefore, θ_m and L_b were measured, with the contact arc length being shortened by changing the wheel diameter D from 200 to 140 mm.

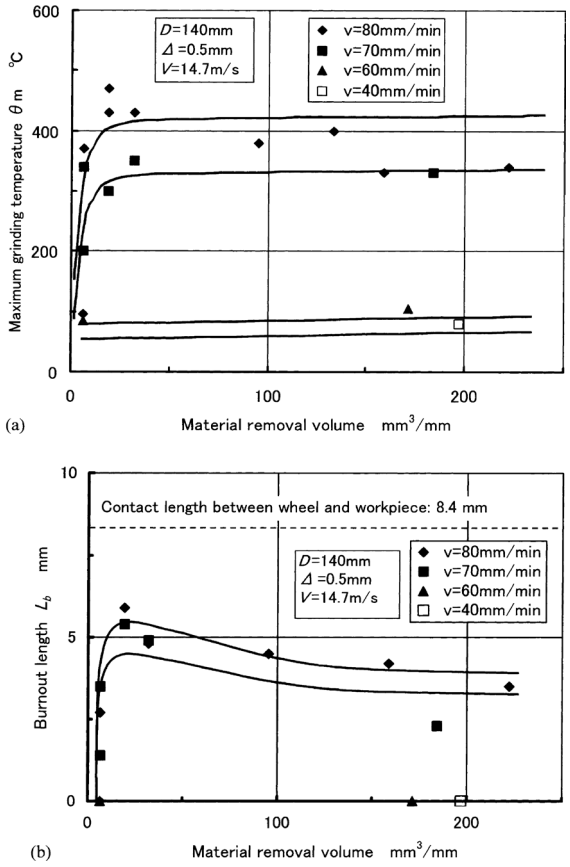

Figure 5. Influence of worktable speed v on the maximum grinding temperature θm and burnout length Lb for wheel diameter D = 140 mm. (a) Changes in θm with material removal volume. (b) Changes in Lb with material removal volume

The results are shown in Figure 5. It is obvious that the variations in θ_m and L_b are almost the same as in Figure 4, and that the length of the region where the cooling effect of the grinding fluid remains good in the contact arc is almost the same at 3 mm. However, the ratio of L_b to the total length of the contact arc becomes greater as the wheel diameter decreases, and the cooling effect of the grinding fluid increases. As a result, where burnout occurred under conditions of V =14.7 m/s, Δ = 0.5 mm, and v = 60 mm/min at D = 200 mm, it could be avoided if the diameter was made smaller to D = 140 mm for example. Thus, making the wheel diameter smaller is one method of increasing the cooling effect of the grinding fluid.

In the grinding of cermet, it is generally recommended to select a low wheel speed to reduce the generation of grinding heat. The same experiments were carried out at higher wheel speeds of 29.3 and 41.9 m/s, and the grinding temperature distribution and the maximum grinding temperature θ_m were measured. After the grinding temperature appeared reach a steady state, after removing 200 mm^3/min, the distributions were compared, as shown in Figure 6.

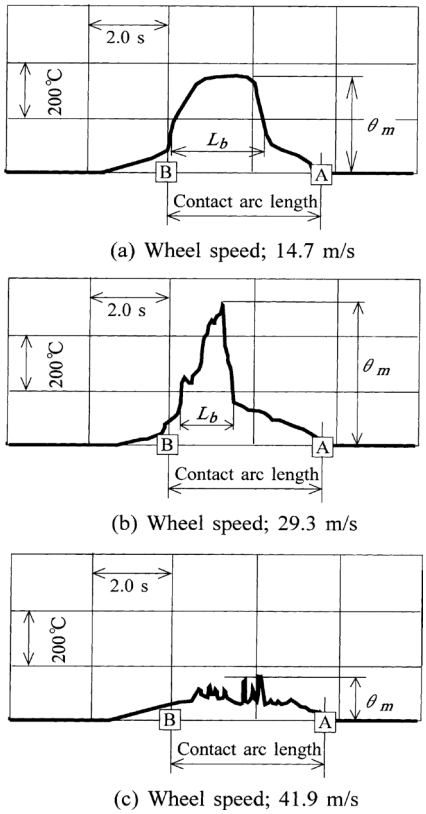

Figure 6. Comparison of grinding temperature distributions along contact arc (D = 200 mm, D = 0.5 mm, v = 80 mm/min, material removal volume: 200 mm^3/mm)

Figure 7(a) and (b) show the changes in θ_m and L_b with material removal volume at wheel speeds of 14.7, 29.3, and 41.9 m/s. The temperature θ_m for V = 29.3 m/s becomes higher than for V = 14.7 m/s, and burnout began to occur at an early stage of grinding. However, the burnout length became shorter and the length of the section where the cooling effect of grinding fluid exists in the contact arc

reached approximately 6 mm (60% of the total length of the contact arc), which is more extensive than for $V = 14.7$ m/s. This indicates that despite the initially elevated maximum temperature, the spatial extent of effective fluid cooling is substantially improved at intermediate wheel speeds. Furthermore, at the higher wheel speed of $V = 41.9$ m/s, burnout almost never occurs and θ_m remains below 150°C along the entire contact arc, demonstrating that the critical burnout threshold is not exceeded throughout the measurement period. The progressive reduction in burnout length with increasing wheel speed confirms that fluid entrainment and transport through the contact zone are enhanced at higher peripheral velocities. Thus, it was demonstrated that higher wheel speed results in an increase in the cooling effect of grinding fluid, a result that is contrary to conventional expectations and is explained by the increased velocity of fluid movement through the grinding zone, which limits the time available for film boiling to develop at any given location along the contact arc.

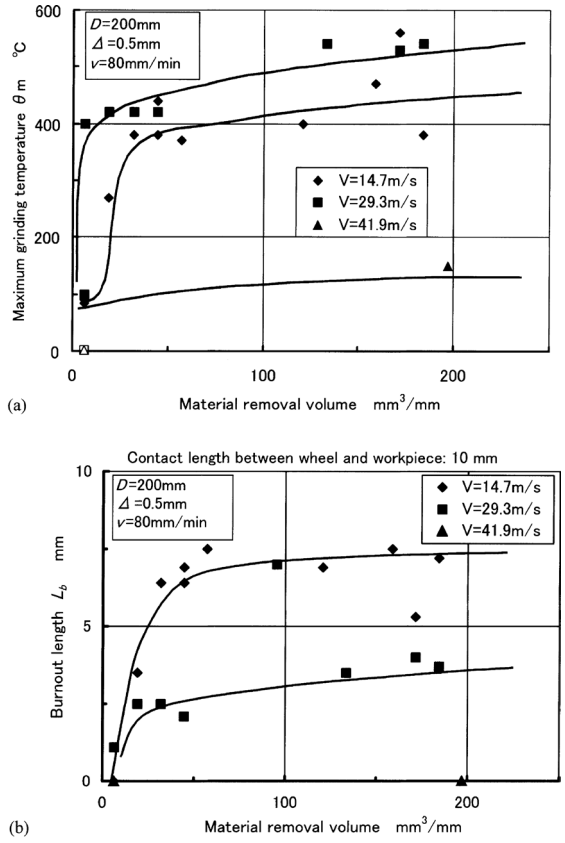

Figure 7. Influence of wheel speed V on maximum grinding temperature θ_m and burnout length L_b. Changes in (a) θ_m and (b) L_b with material removal volume

Figure 8 schematically illustrates how the grinding heat generated in the contact arc between the wheel and workpiece transfers to a film of grinding fluid, in which bubbles are generated and grow due to boiling. Assuming that the time to reach the burnout state is not noticeably influenced by wheel speed V and is almost constant, then the greater the value of V, the faster the movement of the grinding fluid. Therefore, the region where the cooling effect of grinding fluid is available within the contact arc between the wheel and workpiece will become longer at higher wheel speeds, and it can be considered that the burnout length becomes shorter [7]. Thus by increasing V, it has been found that it is possible to increase the effective cooling effect of grinding fluid [14].

Next, further grinding tests with a still higher wheel speed of $V = 62.9$ m/s were carried out. However, severe burnout occurred within the entire contact arc, and thermal cracks were created on the ground surface immediately after starting grinding and it became impossible to continue.

This appears to be because the generated grinding heat increases and the quantity of grinding fluid supply to the contact arc decreases due to the air flow around the wheel surface at such a high wheel speed.

The schematic captures the essential physical mechanism underlying the burnout phenomenon: as heat flux from the grinding interface exceeds the critical threshold, the fluid film transitions from nucleate boiling to film boiling, effectively creating an insulating vapor layer that dramatically reduces heat extraction capacity. Assuming that the time to reach the burnout state is not noticeably influenced by wheel speed V and is almost constant, then the greater the value of V, the faster the movement of the grinding fluid. Therefore, the region where the cooling effect of grinding fluid is available within the contact arc between the wheel and workpiece will become longer at higher wheel speeds, and it can be considered that the burnout length becomes shorter. The schematic further highlights that fluid entering at the front of the contact arc (supply side A) remains in the nucleate boiling regime over a progressively longer arc length as wheel speed increases, while the vapor film region correspondingly recedes toward the rear of the contact zone. This spatial redistribution of boiling regimes directly explains the experimental observations reported in Figure 7, wherein increasing wheel speed from 14.7 to 41.9 m/s substantially reduced both maximum grinding temperature and burnout length. Thus, by increasing V, it has been found that it is possible to increase the effective cooling effect of grinding fluid.

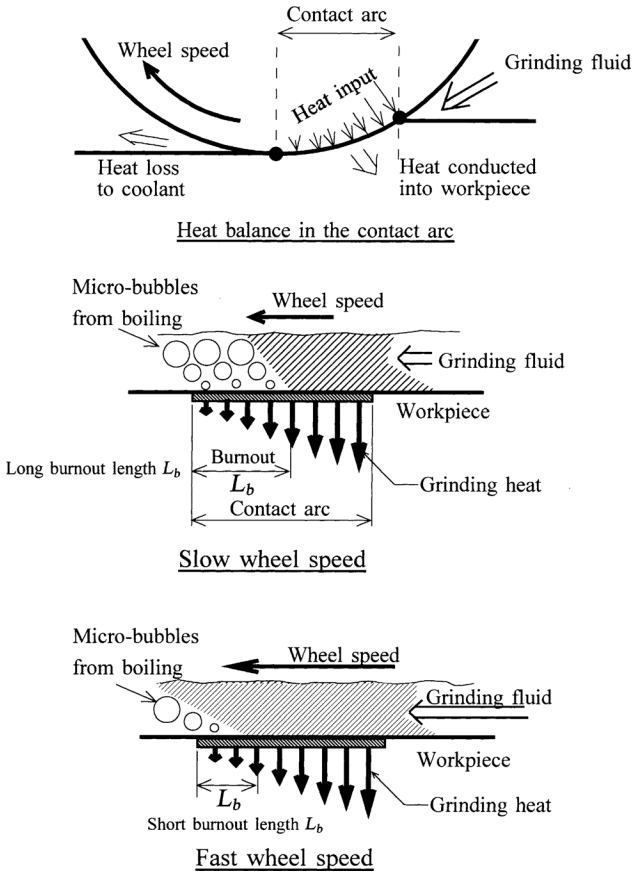

Figure 8. Schematic illustrations of grinding heat transmission from contact arc to grinding fluid

During grinding, normal and tangential grinding forces were measured using a piezoelectric dynamometer mounted on the worktable. The changes in the normal grinding force F_n with material removal volume at various wheel speeds V are shown in Figure 9. It is clear from the figure that the value of F_n decreases with increasing wheel speed, and that F_n becomes constant at $V = 41.9$ m/s, under which burnout almost never occurs along the entire contact arc. At V = 14.7 and 29.3 m/s, however, F_n suddenly increases at the early stages of grinding due to the burnout explained in the previous section. This abrupt force escalation at lower wheel speeds is directly attributable to the thermal expansion of the workpiece material in the vicinity of the grinding point, which effectively increases the grain depth of cut and promotes accelerated fracture and pullout of abrasive grains from the wheel bond. The progressive grain loss under burnout conditions leads to a reduction in the number of active cutting edges, forcing the remaining grains to sustain disproportionately higher individual cutting loads, thereby amplifying the measured normal force. By contrast, at $V = 41.9$ m/s, where burnout is effectively suppressed, the grinding interface remains thermally stable throughout the material removal process, preserving both the wheel topography and the cutting efficiency of individual abrasive grains. The resulting force stability at this optimal wheel speed confirms that thermal management through wheel speed optimization is not only beneficial for surface integrity but also directly governs the mechanical loading experienced by the grinding wheel, with consequent implications for wheel life and process reliability.

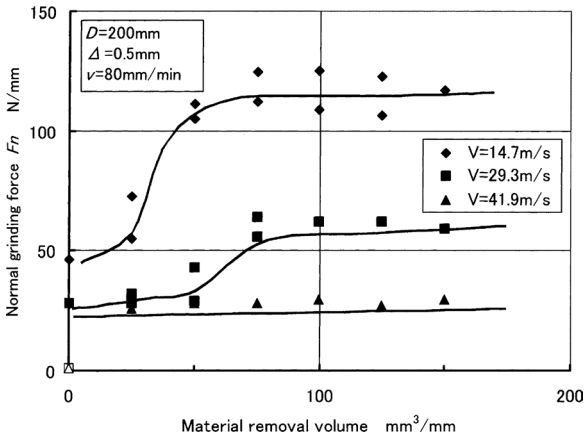

Figure 9. Comparison of normal grinding force F_n for various wheel speeds V

Figure 10 shows the relationship between radial wheel wear Wr and grain cutting length l at various wheel speeds V. The dot-dash lines in the figure indicate the same material removal volume points. It is clear from the figure that higher wheel speed causes a reduction in the wheel wear rate and Wr was reduced. This is probably due to the combined effect of the decrease in cutting force per effective cutting edge due to the high wheel speed, and the increased cooling effect of the grinding fluid. The relationship between Wr and grain cutting length reveals that at lower wheel speeds, where burnout conditions prevail, the wear progression is characteristically nonlinear, with an accelerated initial wear phase corresponding to the onset of thermal damage within the contact arc. This nonlinear behavior is consistent with the abrupt increase in normal grinding force F_n documented in Figure 9, wherein thermally induced grain fracture and bond degradation collectively accelerate material loss from the wheel working surface. At higher wheel speeds, and particularly at V = 41.9 m/s where burnout is effectively eliminated, the wear curve exhibits a more gradual and linear progression with respect to grain cutting length, indicative of a stable and predictable attritious wear mechanism rather than catastrophic grain pullout. The suppression of burnout at optimal wheel speed therefore yields a dual benefit: not only is the grinding interface maintained at thermally safe temperatures, but the structural integrity of the diamond abrasive layer is preserved over extended grinding intervals, resulting in significantly improved wheel life and more consistent

workpiece surface quality throughout the operational lifespan of the grinding wheel.

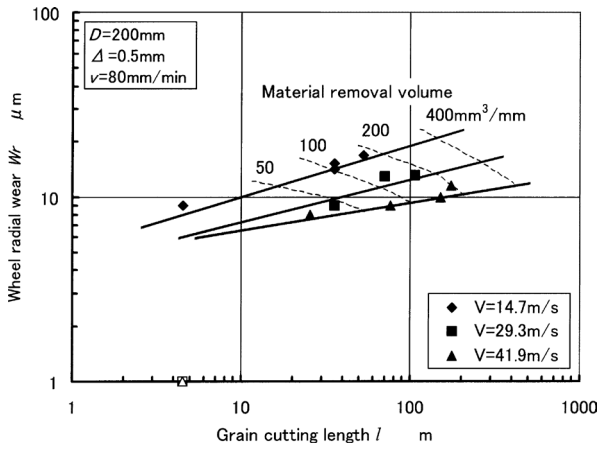

Figure 10. Comparison of wheel radial wear *Wr* for various wheel speeds *V*

4. Conclusions

Creep-feed grinding tests were carried out on cermet, which is extremely difficult to grind, and the grinding temperature distribution along the contact arc between the wheel and the workpiece was measured. Changes in the distribution during grinding were also observed, and the influences of worktable speed, wheel diameter and wheel speed on the maximum grinding temperature were investigated. The results are as follows:

(i) The grinding temperature along the contact arc is lowest on the supply side of the grinding fluid, below 100°C, and higher on the opposite side. When the temperature reaches approximately 150°C, burnout occurs and the temperature rises suddenly to 400°C or more. In other words, even if grinding fluid is being supplied, a similar state to dry grinding appears in the contact arc between the wheel and the workpiece.

(ii) Burnout starts from the rear of the contact arc and extends almost throughout the contact arc as grinding progresses.

(iii) When the depth of cut and the wheel speed are made constant, there exists a critical worktable speed at the boundary of burnout and non-burnout.

(iv) The length of the burnout region can be shortened by using a smaller wheel diameter.

(v) The length of the burnout region can be made smaller if the wheel speed is increased. At the wheel speed of V = 41.9 m/s, burnout almost never occurs and θ_m remains below 150°C along the entire contact arc.

(vi) The faster the wheel speed, the smaller the grinding force and hence wheel wear.

References

[1] Aramian, A., Sadeghian, Z., Narimani, M., Razavi, N., Berto, F.: A review on the microstructure and properties of TiC and Ti(C,N) based cermets. International Journal of Refractory Metals and Hard Materials. 115, 106320 (2023). https://doi.org/10.1016/j.ijrmhm.2023.106320.

[2] Ragothuman, A., Kanthi Natarajan, G.V., Shanmugavel, B.P.: Wear and thermal stability of TiCN-WC-Co-Cr3C2 cermets modified by TiN. International Journal of Refractory Metals and Hard Materials. 84, 105020 (2019). https://doi.org/10.1016/j.ijrmhm.2019.105020.

[3] Yin, Y., Chen, M.: Analysis of Grindability and Surface Integrity in Creep-Feed Grinding of High-Strength Steels. Materials. 17, (2024). https://doi.org/10.3390/ma17081784.

[4] Miao, Q., Li, H.N., Ding, W.F.: On the temperature field in the creep feed grinding of turbine blade root: Simulation and experiments. International Journal of Heat and Mass Transfer. 147, (2020). https://doi.org/10.1016/j.ijheatmasstransfer.2019.118957.

[5] Dai, C.-W., Ding, W.-F., Zhu, Y.-J., Xu, J.-H., Yu, H.-W.: Grinding temperature and power consumption in high speed grinding of Inconel 718 nickel-based superalloy with a vitrified CBN wheel. Precision Engineering. 52, 192–200 (2018). https://doi.org/10.1016/j.precisioneng.2017.12.005.

[6] Ortega, N., Bravo, H., Pombo, I., Sánchez, J.A., Vidal, G.: Thermal Analysis of Creep Feed Grinding. Procedia Engineering. 132, 1061–1068 (2015). https://doi.org/10.1016/j.proeng.2015.12.596.

[7] Heinzel, C., Kolkwitz, B.: The Impact of fluid supply on energy efficiency and process performance in grinding. CIRP Annals. 68, 337–340 (2019). https://doi.org/10.1016/j.cirp.2019.03.023.

[8] Brinksmeier, E., Aurich, J.C., Govekar, E., Heinzel, C., Hoffmeister, H.-W., Klocke, F., Peters, J., Rentsch, R., Stephenson, D.J., Uhlmann, E., Weinert, K., Wittmann, M.: Advances in Modeling and Simulation of Grinding Processes. CIRP Annals. 55, 667–696 (2006). https://doi.org/10.1016/j.cirp.2006.10.003.

[9] Pang, J., Wu, C., Li, B., Zhou, Y., Liang, S.Y.: Experimental Investigation Of The Real Contact Arc Length Measurement In The Cylindrical Plunge Grinding. MATEC Web Conf. 67, 05023 (2016). https://doi.org/10.1051/matecconf/20166705023.

[10] Ito, Y., Kita, Y., Fukuhara, Y., Nomura, M., Sasahara, H.: Development of In-Process Temperature Measurement of Grinding Surface with an Infrared Thermometer. Journal of Manufacturing and Materials Processing. 6, (2022). https://doi.org/10.3390/jmmp6020044.

[11] Vogt, C., Babariya, G., Kukso, O.: An experimental approach to temperature measurement in the contact zone when grinding brittle-hard materials. In: Eleventh European Seminar on Precision Optics Manufacturing. pp. 87–95. SPIE (2024). https://doi.org/10.1117/12.3030935.

[12] Yi, J., Jin, T., Zhou, W., Deng, Z.: Theoretical and experimental analysis of temperature distribution during full tooth groove form grinding. Journal of Manufacturing Processes. 58, 101–115 (2020). https://doi.org/10.1016/j.jmapro.2020.08.011.

[13] Krajnik, P., Wegener, K., Bergs, T., Shih, A.J.: Advances in modeling of fixed-abrasive processes. CIRP Annals. 73, 589–614 (2024). https://doi.org/10.1016/j.cirp.2024.05.001.

[14] Lopez-Arraiza, A., Castillo, G., Dhakal, H.N., Alberdi, R.: High performance composite nozzle for the improvement of

cooling in grinding machine tools. Composites Part B: Engineering. 54, 313–318 (2013). https://doi.org/10.1016/j.compositesb. 2013.05.029.
[15] Hou, Z., Yao, Z.: Investigation on grinding temperature and heat flux distribution with grooved grinding wheels. Int J Adv Manuf Technol. 124, 3471–3487 (2023). https://doi.org/10.1007/s00170-022-10679-1.
[16] Paknejad, M., Abdullah, A., Azarhoushang, B.: Effects of high power ultrasonic vibration on temperature distribution of workpiece in dry creep feed up grinding. Ultrasonics Sonochemistry. 39, 392–402 (2017). https://doi.org/10.1016/j.ultsonch.2017.04.029.
[17] Qin, B., Liu, H., Cheng, J., Tian, J., Sun, J., Chen, G., Yang, Z., Chen, M.: Material removal mechanism in ultra-precision grinding of hard and brittle materials using small ball-end diamond grinding wheel. Journal of Materials Processing Technology. 343, 118977 (2025). https://doi.org/10.1016/j.jmatprotec.2025.118977.
[18] Li, Z., Zhang, F., Luo, X., Guo, X., Cai, Y., Chang, W., Sun, J.: A New Grinding Force Model for Micro Grinding RB-SiC Ceramic with Grinding Wheel Topography as an Input. Micromachines. 9, (2018). https://doi.org/10.3390/mi9080368.
[19] Barmouz, M., Steinhäuser, F., Azarhoushang, B., Khosravi, J.: Influence of bond thermal and mechanical properties on the additively manufactured grinding wheels performance: Mechanical, wear, surface integrity, and topography analysis. Wear. 538–539, 205215 (2024). https://doi.org/10.1016/j.wear.2023.205215.